Partly-Isolated DC-DC Converter for DC Bus Battery-PV Solar Energy System

Vo Thanh Vinh[1], Nguyen The Vinh[2], and Le Van Dai[3,*]

ARTICLE INFO

Article history:
Received: 21 April 2021
Revised: 16 June 2021
Accepted: 22 June 2021

Keywords:
Three-port DC-DC converter
Bidirectional buck-boost
Photovoltaic (PV) panel
Maximum power point tracking control (MPPT)
Simultaneous power management
PSIM software

ABSTRACT

A partly-isolated three-port DC-DC converter for simultaneous power management of multiple energy sources is investigated in this paper. The converter topology composes of a bidirectional buck-boost and a flyback isolated switched-capacitor through a bidirectional converter. This proposed converter is the capability of interfacing sources of different voltage-current characteristics with a DC-link and/or a load. The proposed converter is applied for simultaneous power management of energy sources as photovoltaic (PV) panel, battery, and DC-link and/or load. The operation of the converter is based on a combination of three switches with four states that are created as a binary variable. It is necessary to set input generation sources and output voltage through various control variables to control the converter in each state. The effectiveness of the proposed converter is verified via simulation based on PSIM software and through experiments. The obtained results show that the converter is not only capable of maximum power point tracking control (MPPT) for the PV panel when there is solar radiation, more also can control the charge or discharge of the battery by its characteristic.

1. INTRODUCTION

The use of solar energy is only limited by human ingenuity. There can apply it in fields such as space heating and cooling through solar architecture, drinking water distillation and disinfection, daylighting, solar hot water, solar cooking, and high-temperature thermal processes for industrial purposes. Most importantly, solar energy can convert into electrical energy. Today, solar photovoltaic, using power electronics systems, has changed the image for utilizing solar energy [1]. The cost of solar cells with technology is getting cheaper [2]. However, there are still issues concerning the efficiency of the photovoltaic panels and the process of converting energy to the grid and load. The output voltage of low-power renewable energy sources is usually low wherefore it must use a DC-DC converter to increase the voltage and a DC-AC converter to connect with the power grid. The series connection of the above two converters is the DC-DC-AC multiplier converter that connects between the renewable energy sources the load or AC grid. Therefore, a high boost ratio DC-DC converter has many effects on the overall efficiency of the system [3-6]. The DC-DC boost-flyback converter cannot apply in high boost ratio applications due to some limitations. For example, the duty cycle in a boost circuit increases to be close to 1 for high DC voltage gain resulting in the limited parameters in the circuit as the power switch element, coil, capacitor. This happens because of encountering electromagnetic interference and reverse-recovery issues at extreme duty cycles. Moreover, the large cause of power loss of the main switch is the energy leakage of the primary and secondary winding in the pulse transformer of the boost-flyback converter. Besides, the number of decentralized energy sources is continuously growing. So that it negatively affects the quality of the grid voltage [7, 8].

Nowadays, large amounts of the distributed energy sources are connected to the existing grid resulting in the effect of power quality in the connected area. The deterioration in power quality may result in the loss of connecting the DC-AC converter with the grid. So that is because the power quality is outside the set range of the inverter resulting in disability to feed power to the grid. In addition, the grid's power quality is not only the cause of the unreliable PV power generation system but also loads (electricity customers) experiencing a higher than rated grid voltage. To overcome the above problems, a lot of researches have been proposed effective solutions to improve the characteristic of the boost converter. For

[1]*Dong Thap University, Dong Thap, Viet Nam*
[2]*International Francophone Institute, Vietnam National University, Hanoi, Viet Nam*
[3]*Faculty of Electrical Engineering Technology, Industrial University of Ho Chi Minh City, Ho Chi Minh City, Viet Nam.*
**Corresponding author:* Le Van Dai; Email: levandai@iuh.edu.vn.

example, a switch with capacitors has been introduced in [9-13], the coupling inductor has been presented in [14-19], and the increased voltage is introduced in [20, 21]. The authors in [22] have proposed a DC-DC converter bidirectional multi-level in the power system DC sources. In this study, the output level can be changed almost continuously without any magnetic components. One of the major benefits of this magnetic-less system is that very high-temperature operation is possible in comparison to conventional solutions.

In [23], the authors have proposed a new bidirectional non-isolated three-port DC-DC converter is developed from the bidirectional DC-DC converter base boost and buck. The direct conversion energy is better performance. In this architecture, the converter is connected between the PV source pack, the battery pack, and the DC-link. In this case, the switching power of the converter is large voltage stress with the scenario of boost condition. In [24], the authors have proposed a single-inductor dual output switching converter topology that can independently regulate two output voltages; besides, the proposed solution use only one inductor and make four power switches. In this architecture, it is beneficial due to the reduction of one inductor. The proposed solution in [25] is considered as a further improvement method, in which a three switch DC-DC converter with two outputs is presented. The DC-DC converters bidirectional of high efficiency using soft circuit or parallel switching solutions is proposed in [26-28]. A comparative study shows current advancements in non-isolation bi-directional topologies [29]. Diagrams using two bridge converters with a large number of power switches are suggested, those schemes are suitable for high power and not for small power applications [30]. The use of the nonlinear voltage regulation algorithm for DC-DC boost converter is proposed in [31]. The modulation scheme for switching DC-DC converter is introduced in [32].

Based on the current research situation of the above-mentioned problem as well as the future outlook, this study proposes the bidirectional converter topology composing of a bidirectional buck-boost and a flyback isolated switched-capacitor through a bidirectional converter. The proposed converter is shown in Figure 1. The main contribution of this proposed converter is, for the step-up model, the output voltages of the coupled inductor boost and the switched capacitor are connected in series to obtain a high gain with a high conversion efficiency even under hard-switching mode and even a high conversion efficiency even under hard-switching mode. Thanks to these features, the operating range of the proposed can be broadened. In addition, this proposed converter performs energy storage tasks on the battery and is flexible in the bidirectional process of supplying and receiving battery power and DC-link/load.

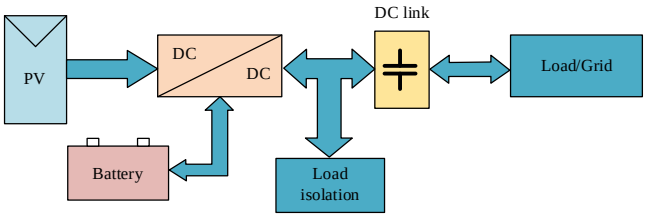

Fig. 1. The proposed DC-DC converter.

This paper consists of four sections with content for each one as Section 1 presents the urgency, settlement, and unresolved for the DC-DC converter problem. The proposed DC-DC-AC converter presents Section 2. The experimental procedures and settings are presented in Section 3. Finally, the conclusion and future research aspects are presented in Section 4.

2. TOPOLOGY AND OPERATING SCENARIOS OF THE PROPOSED CONVERTER

2.1. Topology of the proposed converter

The proposed converter topology is shown in Figure 2, which consists of a low-voltage-side (LVS) circuit and a high-voltage-side (HVS) circuit connected via a high-frequency transformer with a primary winding L_1 two secondary windings L_{21} and L_{22}. The LVS consists of two ports (connected to the PV panel and the battery), a switch M_1, two capacitors C_1 and C_{bat}, the primary and secondary winding of the transformer L_1 and L_{21}, respectively, and two diodes D_1 and D_2. The HVS consists of one port (connected to the DC-link/load), the secondary winding of the transformer L_{22}, two switches M_2 and M_3, two capacitors C_2 and C_3, a diode D_3, and an inductor L_1.

The presented structure utilizes a unidirectional power switch (M_1) and two bidirectional power switches (M_2 and M_3). Among the switches, M_1 is called the main switch because it controls the amount of power generated from the PV system. To simplify the analysis, all capacitances in the circuit are assumed that they have sufficient value such that the voltages across them are constant within a switching period. The pulse width modulation (PWM) strategy for each scenario is explained for the control of the duty cycle that results in the switching of the power switches. The recovery stage is constituted by the diode D_1 and the capacitor C_1 (explanation of the working modes in this recovery stage is fully described in [33]) for four scenarios will be explained in Section 2.1.

The switching states are created based on the binary variable to express the converter operation through a combination of three switches. In this study, the switching states are shown in Table 1 which has eight switching states, and to simplify the analysis, the proposed converter is analyzed by four operation scenarios corresponding to four switching states 5, 7, 3, and 2, namely ST-1, ST-2, ST-3, and ST-4, respectively.

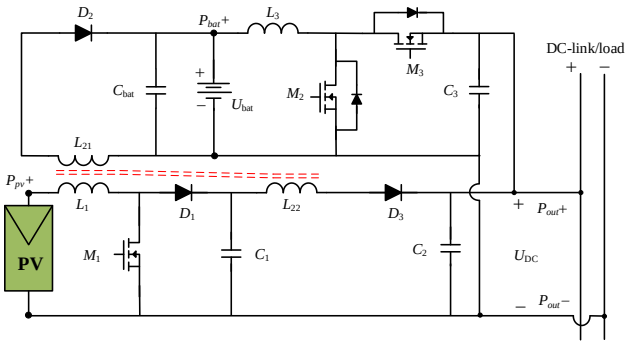

Fig. 2. The proposed bidirectional DC-DC converter.

Table 1. The proposed switching states

State	M_1	M_2	M_3	Topology state
1	0	0	0	Not operation
2	0	0	1	TS-4
3	0	1	0	TS-3
4	0	1	1	-
5	1	0	0	TS-1
6	1	0	1	-
7	1	1	0	TS-2
8	1	1	1	-

2.2. Operating scenarios

Case 1: Topology state 1 (TS-1), in this case, the resonant circuit structure is the one-input and two-output type as shown in Figure 3. This case will operate when the PV is exposed to sunlight and becomes the source of energy for charging energy to the battery, supplying energy to the DC-link/load, and dissipating energy on the inductors L_1, L_{21}, and L_{22}. This state usually occurs during the daytime when there is maximum sunlight. The gate signal with the duty ratio (d_1) is applied to M_1, meanwhile, M_2 and M_3 are turned OFF. When the converter operates in the steady-state, four operating modes depending on the switching period of M_1, and the steady-state waveforms of the four modes are depicted in Figure 4.

Mode 1: $t \in [t_0, t_1]$: M_1 is ON, the coupled inductors work in the flyback and boost states to store the energy from the PV. The output of rectifier diodes D_2 and D_3 are reverse-biased leading to the currents through i_{D_2} and i_{D_3} are zero. Due to the leakage inductor of L_1, the secondary-side currents through inductors $i_{L_{21}}$ and $i_{L_{22}}$ are zero. The stored energy in capacitor C_2 transfers to the DC-link/load and the stored energy in capacitor C_{bat} transfers to the battery.

Mode 2: $t \in [t_1, t_2]$: M_1 is OFF at t_1, while the diodes D_1, D_2, and D_3 are forward-biased. The energies of the leakage inductor L_1 and the magnetizing inductor L_1 are released to charge the clamp capacitor C_1 via the rectifier diode D_1. Therefore, the energy of L_{21} and L_{22}, and PV transfer to the output DC-link/load and battery. At t_2, the capacitor C_1 charges full, the leakage inductor of L_1 current decreases due to the existence of L_{22}.

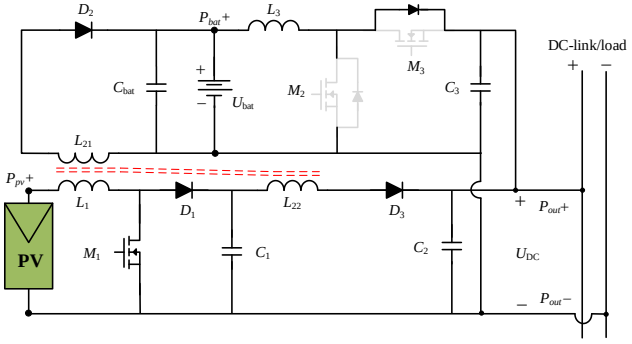

Fig. 3. The topology of the proposed converter under operating TS -1.

Mode 3: $t \in [t_1, t_2]$: At t_2, M_1 is OFF, the diodes D_1, D_2, and D_3 is ON. The energy of secondary-side windings of the coupled inductor L_{21} and L_{22}, and capacitor C_1 transfer to the DC-link/load and battery. At t_3, the energy leakage inductor L_1 is zero, the energy of the capacitor C_1 discharges to the L_{22}.

Mode 4: $t \in [t_1, t_2]$: Continuing Mode 3, the energy of the DC-link/load and the battery is taken from capacitors C_1 and secondary-side windings L_{21}, L_{22}. The increased output voltage is due to the energy stored windings in the transformer. Along with the self-inductance, mutual between the windings and frequency of main power switch M_1.

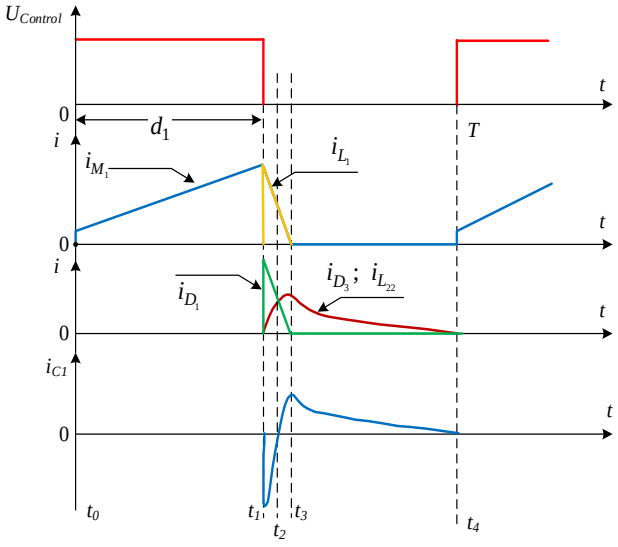

Fig. 4. The waveforms of the proposed converter under operating TS -1.

The converter operates as a flyback and a coupling magnetic boost converter. The flyback converter is the turn ratio of $N_1 = n_{21} / n_1 > 1$ (where n_1 and n_{21} are the numbers of turns of L_1 and L_{21}, respectively), with the aim is to increase the voltage (the reason is that the battery voltage is greater than the PV voltage). This leads to the increased efficiency during the charge for the battery, and it can satisfy the following condition

$$U_{DC-link} > U_{Bat} > U_{PV} \quad (1)$$

Furthermore, the connection of the proposed converter for the systems with isolated loads is not affected the whole system. The boost converter is the turn ratio $N_2 = n_{22} / n_1 > 1$ (where n_{21} is the number of turns L_{22}). Besides, when the battery is fully charged, the energy from PV continues transferring to the DC-link by coupling a magnetic boost.

The proposed converter, operating in this case, can be made from the isolation circuit that has just been charged to the battery.

Case 2: Topology state 2 (TS-2), in this case, the resonant circuit structure is the two-input and two or one-output type as shown in Figure 5. The power is transferred from PV to the DC-link/load. The battery is charged fully, the D_2 is OFF. The D_2 has not only one task for rectifying current and voltage from the output of L_{21} but also cutting out the battery when the battery is fully charged. It does not matter to the control mode in the converter. Therefore, this is also a solution to simplify the control circuit. In this converter structure, the isolated circuit uses the charging characteristics of the battery to calculate the L_{21} winding value, and the voltage on the top of the two windings is considered constant. The amount of energy is charged to the battery depends on the increased voltage [34-35]. So, it is required to discharge the energy from the battery to supply the needed. The converter is directly derived from common and well-known boost as operation boost basic and boost coupling magnetic topologies as TS-1. In applications where high voltage gain is required, boost coupling magnetic topologies typically imply improved performance and efficiency [33,36-37].

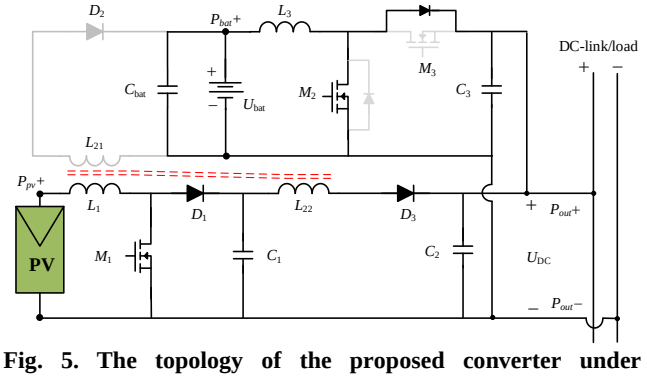

Fig. 5. The topology of the proposed converter under operating TS -2.

In this case, the switches M_1 and M_2 are operating, M_3 is not operating. Two gate signals with the duty ratios of d_1, d_2 are applied to M_1 and M_2. At the time that the battery is fully charged and the diode D_2 is reverse-biased. So, the inductor L_{21} is an open circuit in this state. When the battery discharges, its voltage is less than the voltage on $L_{21:2}$ [34-35], and next period, the state will change the same as *Case* TS-1 as shown in Figure 6.

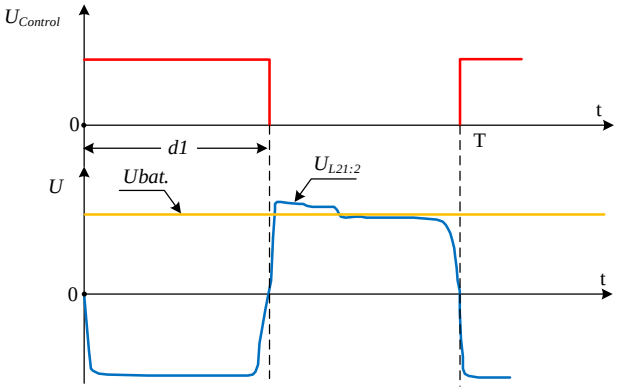

Fig. 6. The waveforms of the voltage under operating TS -2.

Case 3: Topology states 3 and 4 (TS-3 and -4), in this case, the circuit diagram of the proposed bidirectional converter (BC) is given in Figure 7.

For state ST-3, the energy of the battery transfer to the DC-link/load as shown in Figure 7, the converter works as a boost converter, in which the M_2 is operating, the M_1 and M_3 are not operating. The source of energy is provided by the battery that has been maintained at a specific voltage during two operation states. This case is operating during low light conditions when the power generated from the PV panel is very low. In this case, L_3 will be charged/discharged. For state *TS-4*, the energy in the battery is reduced to the smallest value, the PV does not provide the energy and at the time, the energy in the DC line is connected to other renewable energy sources that are redundant, leading to the battery being charged the energy from the DC line.

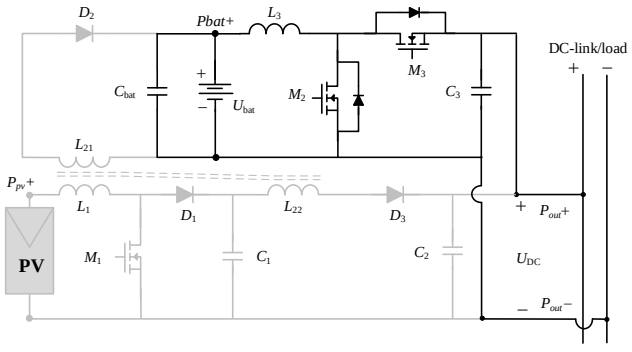

Fig. 7. The topology of the proposed converter under operating TS -3 and 4.

2.3. Control strategy

As described above, the proposed converter can operate in four states. It is necessary to set input generation sources and output voltage through various control variables to control the converter in each state. The primary aim of this paper is to maximize the energy from the PV [38-40] and minimize the energy drawn from the grid. In this case, the status that the battery is rechargeable from DC-link is called a load on the DC-link. The control scheme makes sure that the battery voltage is maintained along with a constant DC-link voltage. Since the source of energy is not constant, several modes can be made in terms of the control aspect to achieve the two goals mentioned above.

This proposed converter is very convenient in the control design combined with feedback loops. So that the power level can be optimized by alternating as discussed in the previous section. Therefore, equations in each mode in each scenario are also considered simply. The states of the four switches M_1, M_2, and M_3 are controlled with the help of a proportional plus integral controller. The PWM strategy is such that it prohibits the situation of the forbidden states as listed in Table 1. The switching frequency is set at 12,5 kHz. The gate signals for switches are directly controlled by the microcontroller. This is done to avoid the situation of the forbidden states. As a result, the mode pulse width of the four switches is never the same, hence avoiding a short circuit.

For *Case* TS-1, the voltage of the DC-link/load and the battery can be determined as follows, respectively

$$U_{DC-link} = U_{C2} = U_{C3} = U_{PV}\frac{d_1}{1-d_1}(1+N_2)((1+k)/2) \quad (2)$$

$$U_{Bat} = U_{Cbat} = U_{PV}\frac{d_1}{1-d_1}N_1 \quad (3)$$

where N_1 is the turns ratio between n_1 and n_{21}, N_2 is the turns ratio from n_1/n_{22}, and k is the coupling factor of the transformer in the converter.

From condition in Eq. (1), we have

$$N_2 > N_1 \quad (4)$$

The PWM strategy is simple for the switch M_1 by the loop controlled for the capacitor C_2.

For Case TS-2, the DC gain for output DC-link/load isolation can be calculated according to the equation:

$$\frac{U_{DC-link}}{U_{Bat}} = d_2 \quad (5)$$

Comparing the Eqs. (1), (3), and (5) it has two following conditions:

Firstly, if output DC-link/ load is equal:

$$d_2 > d_1 \quad (6)$$

Secondly, if output DC-link/load is different than output isolation less:

$$d_2 \geq d_1 \quad (7)$$

The PWM strategy is the same as the one employed in *Case* TS-1. Here also, the three switches have to avoid a short circuit condition thereby all three switches cannot be ON at any given point in time. The control aspect varies slightly from TS-1. There is additional control for the M_2. In this state, there are three closed-loop controls. As shown in Figure 8, the first loop shows the control strategy for the voltage of capacitor C_2, the output of this controller is given to the gate signal of switch M_1. The second loop is the control for the voltage of capacitor C_3, the output of this controller is given to gate M_2. With additional control of mode for M_2 operation or non-operation is the third effectuated loop.

For *Case* TS-3, the DC gain for DC-link/load output is determined Eqs. 5, 6, and 7. The loop is controlled the same as the second loop in TS-2.

For case TS-4, the DC gain for battery output:

$$\frac{U_{Bat}}{U_{DC-link}} = d_3 \quad (8)$$

The PWM strategy in this state is simple by the fourth loop controlled for the switch M_3 depending on the value of the battery and the value of the parameters in the converter. Thus, the controller simply uses four loops in the four operating states of the converter.

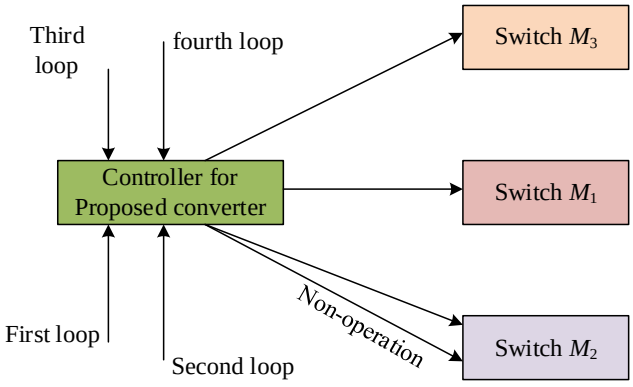

Fig. 8. Diagram of the proposed control scheme.

3. SIMULATION AND EXPERIMENTAL RESULTS

This part gives the simulated and experimental results for each case. The circuit diagram for each state along with the detailed analysis. A comparison between the experimental and simulation results is realized to validate the configuration.

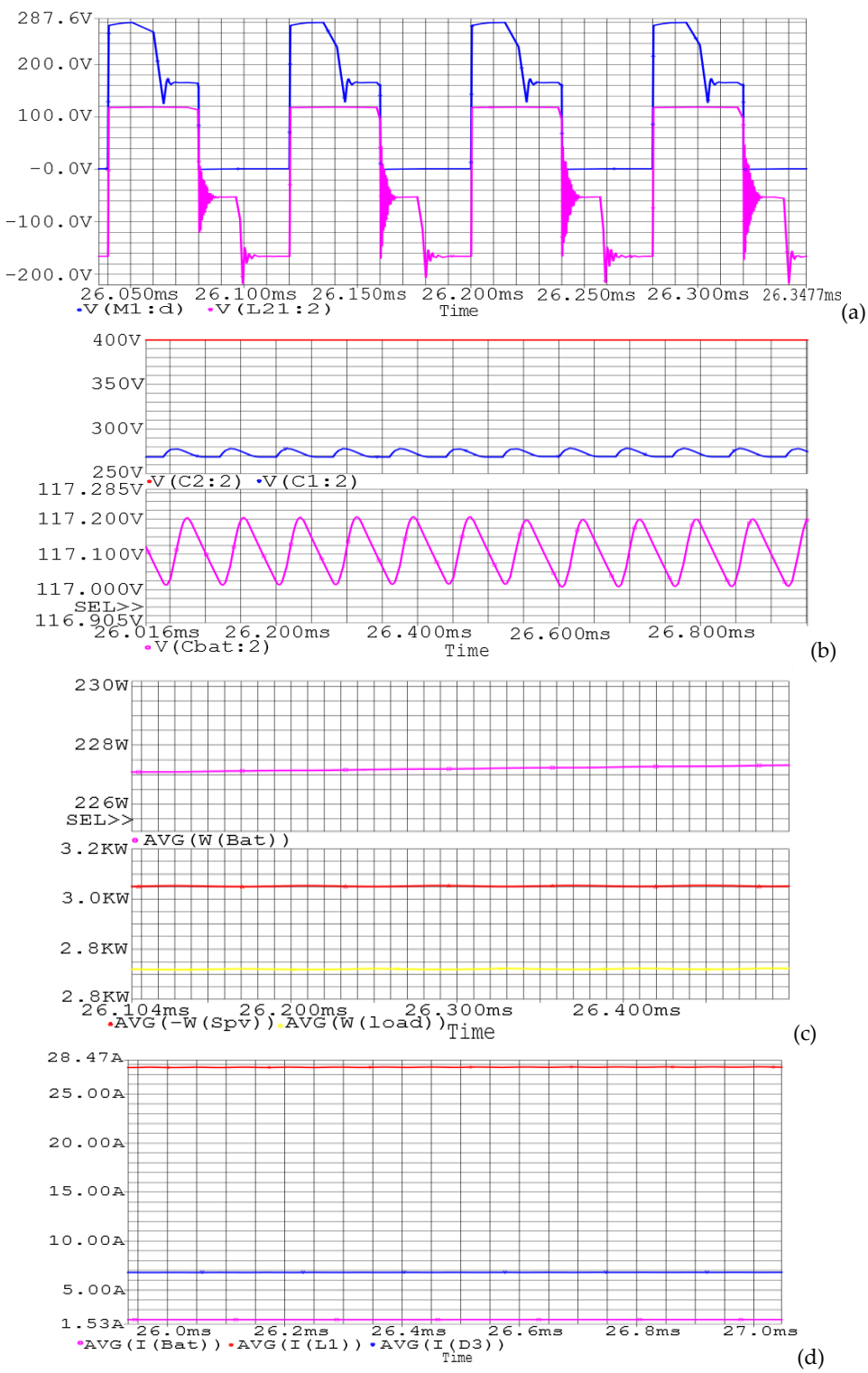

Fig. 9. Simulation results of the operation in *Case TS-1*: (a) Voltage of switch M_1 and D_2, (b) Voltage of the capacitors and DC-link/load, c) Power of the PV, Battery, and DC-link/load, (d) Currents by PV panels, DC-link/load, and battery.

3.1. Simulation Results

The simulations are performed in Orcad software to evaluate the operation of the proposed converter. The parameter values for simulation are the turn ratios of the transformer are $N_1 = 2{,}2$ and $N_2 = 10$; the coupling factor is $k = 0{,}95$; the capacitors are $C_1 = 47$ µF, $C_{bat} = 470$µF, $C_2 = C_3 = 1000$ µF; the consumed power of PV and Battery is (500-3500) W; the voltage of DC-link/load is 400V, the voltage of the battery is 120V. The used power switches

are MOSFET for M_1 to be IRF7799L2, M_2 to be IRFB4137, and M_3 to be IRFH5025.

Figure 9 shows the simulation results of the operation converter in *Case* TS-1. Figure 9 (a) shows the voltage stress waveform of switch M_1, diode D_2. The power switches are chosen according to the voltage stress of the main switches with considering the maximum voltage of the PV from 70 V to110 V. The voltages, crossing the capacitors C_1, C_2, and C_{bat}, are illustrated in Figure 9 (b), in which the value of capacitor C_1 is changed according to the voltage value of the PV. The output voltage of capacitor C_2 is 400V. Figure 9 (c) shows the generated power of the source, load, and battery. The current of the battery, L_1, and D_3 provided by the PV source is shown in Figure 9 (d). Observing this figure shows that the battery is operating at the charging state and the current, flowing from the DC-link/load, has low.

Figure 10 shows the simulated results for *Case* TS-2, in which the voltage stress waveform is proportional to switches M_1 and M_2, the M_2 is controlled by duty ratio condition in Eq. (6) as shown in Figure 10 (a). So, the power switch M_2 is chosen according to voltage stress but other with the selection of the power switch M_1. The average input current of PV and Battery and output current of DC-link of the converter are shown in Figure 10 (b). Figure 10 (c) shows the generated powers of PV, load, and battery sources.

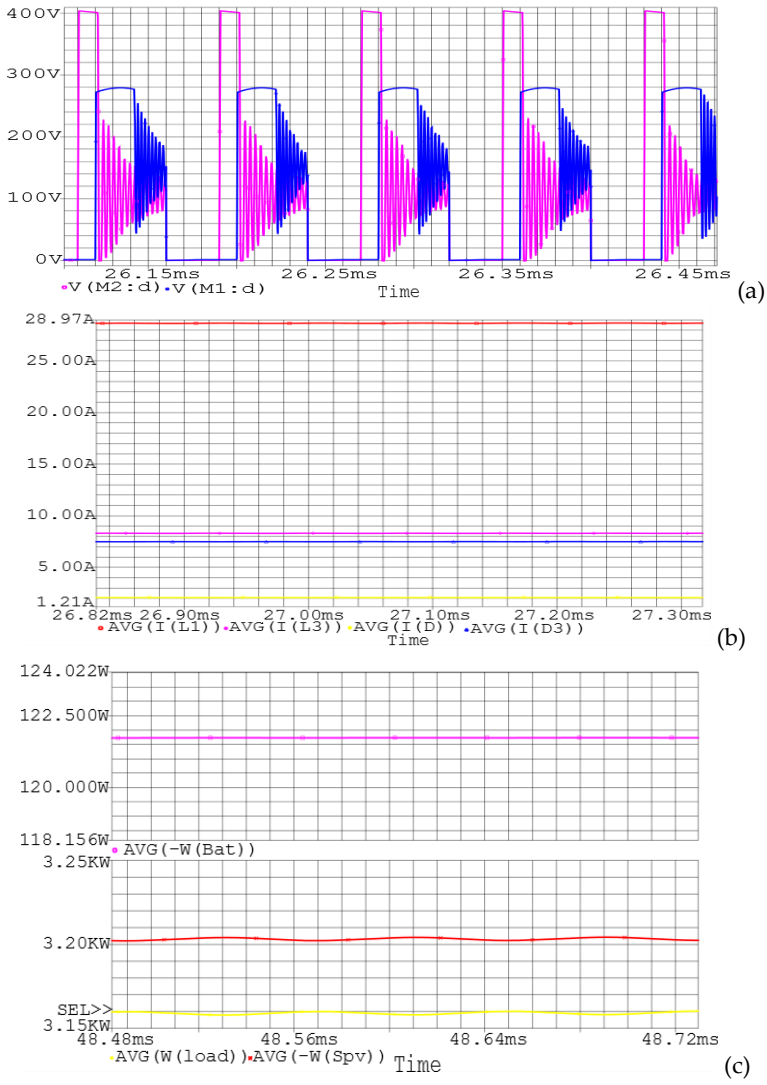

Fig. 10. Simulation results of the operation in *Case TS-2*: (a) Voltage of switch M_1 and M_2; (b) currents of the PV panel, battery, and DC-link; (c) Power of the PV, battery, and DC-link.

For *Case* TS-3, the simulated results are like *Case* TS-2. Figure 11 is illustrated the operation of the proposed converter in *Case* TS-4. The voltage stress waveform proportional to switch M_3 is shown in Figure 11 (a) and the M_3 is controlled by duty ratio condition in Eq. (8). Figure 11 (b) shows the generated powers of the DC-link/load and battery sources.

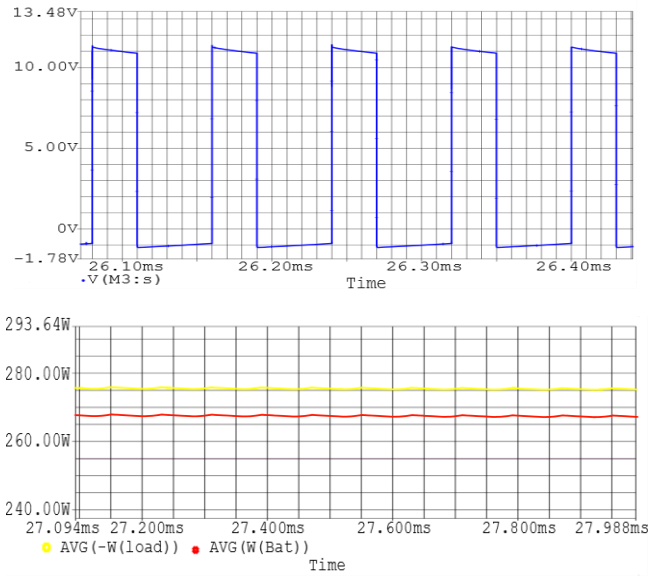

Fig. 11. Simulation results of the operation in *Case TS-4*: (a) The voltage of switch M_3, (b) Power DC-link and battery.

3.2. Experimental Results

The laboratory prototype is equipped for the tests as shown in Figure 12. The PV solar panel is connected to the Battery system via the proposed converter. The converter is connected to the DC-link/load and load isolation as well as the microcontroller. The switches in the converter are connected to the gate drivers. The control circuit for this converter follows the conditions analyzed in Section 2.3. The oscilloscope is used to measure the input and output of the current, voltage, and power under each scenario. The tests are carried out with almost real-world conditions. However, the majority of the laboratory tests were conducted with the use of the resistance load. The converter input (the output of the PV source) is placed in a converted current filter capacitor.

The converter composes of five diodes, four capacitors, and one transformer and it is controlled by three MOSFET switches. This proposed converter can transmit the power smoothly between DC-link/load and the AC grid. The conversion efficiency for the proposed converter is determined by measuring the input and output of the voltage and current under all operation modes for different power levels and PV voltage levels. The experimental results are presented in Figures 13 and 14.

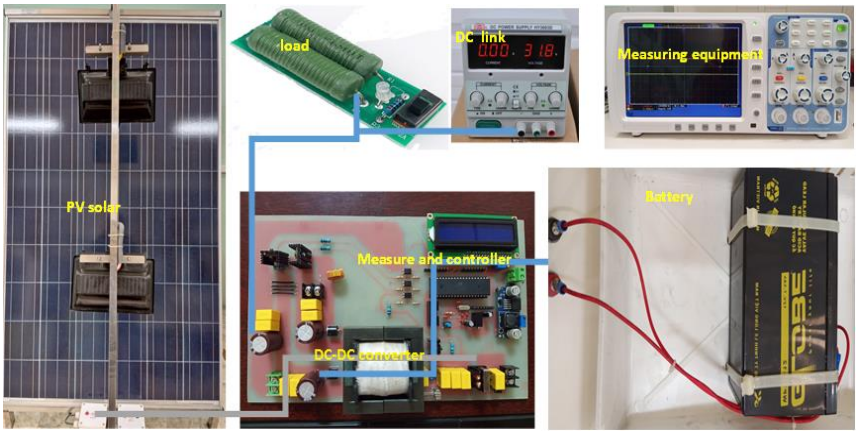

Fig. 12. Hardware picture of the proposed converter.

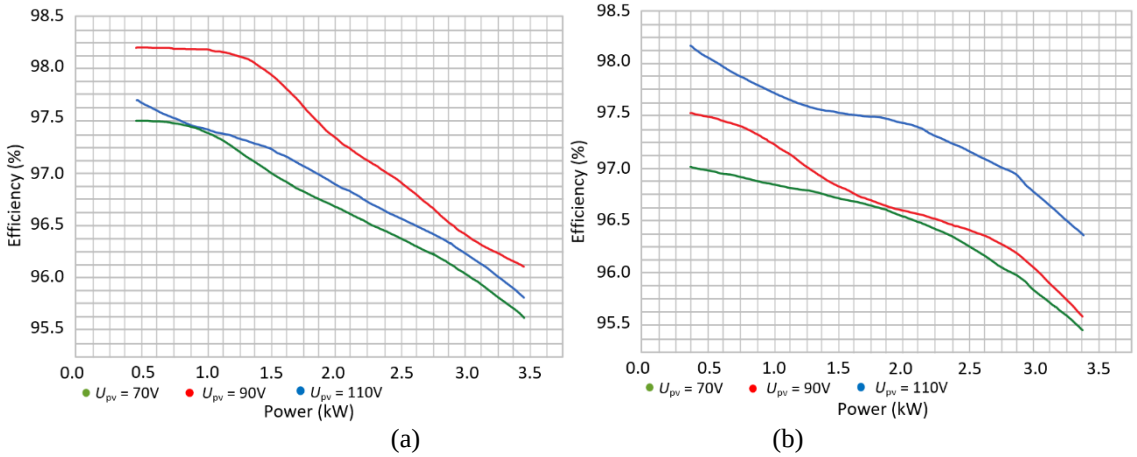

(a) (b)

Fig. 13. Efficiency power of the operation converter: (a) PV to DC-link/load and battery operation, (b) PV and battery to DC-link/load.

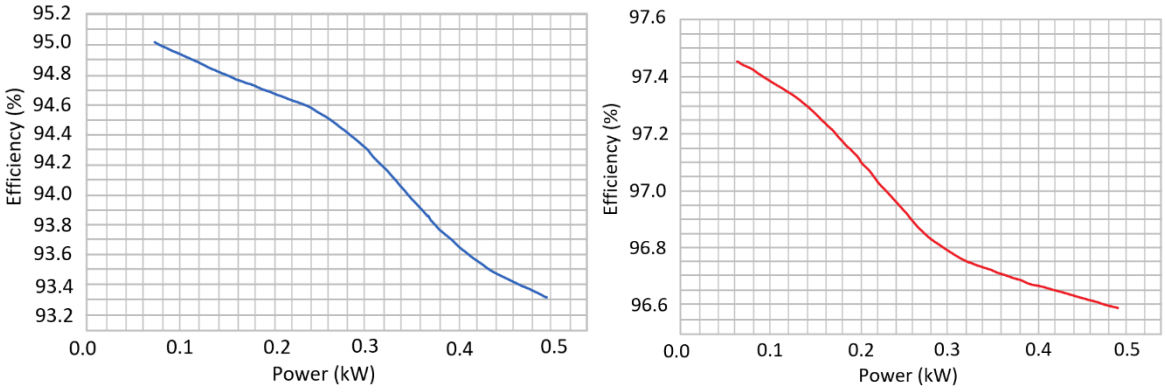

(a) (b)

Fig. 14. Efficiency power of the proposed converter: (a) Battery to DC-link/load and (b) DC-link/load to the battery

Observing the obtained result shows that. The highest efficiencies are measured in the PV to battery operation with a maximum efficiency of 97,8% with *U*pv=110V at 1.2kW and the lowest efficiency of 96% with *U*pv=70V at 2.5kW.

The lowest efficiencies are measured in the battery to the operating DC-link, as shown in Figure 14 (a). Overall, the worst operation case in terms of efficiency is encountered when the converter is operating at high duty cycles for switch M_2, such that the MOSFET has experienced high current stress. Figure 14 (b) shown the efficiency of the results for *Case* TS-4. It can be seen that the maximum efficiency of this converter is 97.5% at 450W and the rated efficiency is approximately 96%.

4. CONCLUSIONS

This study proposed a new partially-isolation, bidirectional DC-DC converter with the least number of switches has been proposed for PV-battery-DC microgrid applications. The proposed topology is suitable for step-up and step-down voltage gains for PV conditioning systems. The topology structure is highly efficient. The simulation and experimental results have shown that the converter is not only capable of maximum power point tracking control (MPPT) for the PV panel when there is solar radiation, more also can control the charge/discharge of the battery by its characteristic.

ACKNOWLEDGMENTS

The authors gratefully acknowledge Dong Thap University, Vietnam National University, Hanoi, and Industrial University of Ho Chi Minh City for the financial support and the facilities offered during this research.

REFERENCES

[1] Lewis, N. S. 2007. Toward cost-effective solar energy use. *Science* 315(5813), pp.798–801.

[2] Renewables 2019 – Global Status Report. REN21 Secretariat, ISBN 978-3-9818911-7-1.

[3] Zhang, L. Sun, K., Feng, L.L., Wu, H.F., Xing, Y. 2013. A family of neutral point clamped full-bridge topologies for transformerless photovoltaic grid-tied inverters. *IEEE Transactions on Power Electronics*, 28(2), pp.730–739.

[4] Duong, M.Q., Le K.H., Grimaccia F., Leva, S., Mussetta, M. 2018. Modeling and performance evaluation of a fuzzy logic controller for buck-boost DC/DC converters. *In 2018 IEEE International Conference on Fuzzy Systems (FUZZ-IEEE*), pp.1–8, July.

[5] Wai, R.J., Duan, R.Y. 2005. High-efficiency power conversion for low power fuel cell generation system. *IEEE Transactions on Power Electronics*, 20, pp. 847–856.

[6] Hsieh, Y.P., Chen, J.F., Liang, T.J., Yang, L.S., 2013. Novel high step-up DC-DC converter for distributed generation system. IEEE Transactions on Industrial Electronics, 60(4), pp.1473–1482.

[7] Cheng, Y., 2010. Impact of large-scale integration of photovoltaic energy source and optimization in smart grid with minimal energy storage. In *2010 IEEE International Symposium on Industrial Electronics*, pp. 3329–3334, IEEE.

[8] Braun, M., Stetz, T., Brundlinger, R., Mayr, C., Ogimoto, K., Hatta, H., Kobayashi, H., Kroposki, B., Mather, B., Coddington, M., Lynn, K., Graditi, G., Woyte, A., MacGill, I., 2016. Is the distribution grid ready to accept large-scale photovoltaic deployment? State of the art progress and future prospects. *Progress in Photovoltaics Researchand Applications*, 20(6), pp. 681–697.

[9] Qian, W., Cao, D., Rivera, J.G.C., Gebben, M., Wey, D. and Peng, F.Z., 2012. A Switched-capacitor DC-DC converter with high voltage gain and reduced component rating and count. *IEEE Transactions on Industry Applications*, 48(4), pp.1397–1406.

[10] Wei, C.L. and Shih, M.H., 2013. Design of a Switched-capacitor DC-DC converter with a wide input voltage range. *IEEE Transactions on Circuits and Systems I*, 60(6), pp. 1648–1656.

[11] Ajami, A., Hossein A., and Amir F. 2015. A novel high step-up DC/DC converter based on integrating coupled inductor and switched-capacitor techniques for renewable energy applications. *IEEE Transactions on Power Electronics*, 30(8), pp. 4255–4263.

[12] Poorali, B., Torkan A., and Adib E., 2015. High step-up Z-source DC-DC converter with coupled inductors and switched capacitor cell. *IET Power Electronics*, 8(8), pp.1394–1402.

[13] Wu, G., Ruan, X. and Ye, Z., 2015. Non-isolated high step-up DC-DC converters adopting switched-capacitor

cell. *IEEE Transactions on Industrial Electronics*, 62(1), pp. 383–393.

[14] Pierre, P., Michel, A., Nguyen, T.V., Charles, J.P., 2014. Basic MOSFET based Vs couple-coils boost converters for photovoltaic generators. *International Journal of Power Electronics and Drive Systems*, 4(1), pp.1−11.

[15] Duong, M.Q., Nguyen, H.H., Nguyen, T.H., Nguyen, T.T., Sava, G.N., 2017. Effect of component design on the DC/DC power converters dynamics. *In2017 10th International Symposium on Advanced Topics in Electrical Engineering (ATEE)*, pp.617−620, Mar. IEEE

[16] Lee, J.H., Liang, T.L., Chen, J.F., 2014. Isolated coupled-inductor-integrated DC-DC converter with nondissipative snubber for solar energy applications. *IEEE Transactions on Industrial Electronics*, 61(7), pp. 3337–3348.

[17] Giang, V.T., Vinh, N.T. and Vinh, V.T., 2018. Highly Efficient step-up Boost-Flyback coupled magnetic integrated converter for photovoltaic energy. *International Journal of Circuit and Electronic*, 3, pp.14–18.

[18] Axelrod, B., Berkovich, Y., 2011. Switched coupled-inductor cell for DC-DC converters with very large conversion ratio. *IET power electronics*, 4(3), pp. 309–315.

[19] Tang, Y., Fu, D., Kan, J. and Wang, T., 2015. Dual switches DC/DC converter with three-winding-coupled inductor and charge pump. *IEEE Transactions on Power Electronics*, *31*(1), pp.461–469.

[20] Chen, Y.T., Tsai, M.H., Liang, R.H., 2014. DC-DC converter with high voltage gain and reduce switch stress. *IET power electronics* 7(10), pp. 2564–2571.

[21] Hu, X. and Gong, C., 2013. A high voltage gain DC–DC converter integrating coupled-inductor and diode–capacitor techniques. *IEEE transactions on power electronics*, *29*(2), pp.789–800.

[22] Shen, M., Peng, F.Z. and Tolbert, L.M., 2008. Multilevel DC-DC power conversion system with multiple DC sources. *IEEE Transactions on Power Electronics*, *23*(1), pp.420–426.

[23] Al-Atrash, H., Tian, F. and Batarseh, I., 2007. Tri-Modal Half-Bridge Converter Topology for three-port interface. *IEEE Transactions on Power Electronics*, 22(1), pp.341−345.

[24] Belloni, M., Bonizzoni, E. and Maloberti, F., 2008. On the design of single-inductor double-output dc-dc buck, boost and buck-boost converters. In *2008 15th IEEE International Conference on Electronics, Circuits and Systems*, pp. 626–629, August, IEEE.

[25] Rojas-Gonzalez, M.A., Torres, J., Sanchez-Sinencio, E. and P. Kumar., 2012. An integrated dual-output buck converter based on sliding mode control. In *2012 IEEE 3rd Latin American Symposium on Circuits and Systems (LASCAS)*, pp.1–4, February, IEEE.

[26] Chen, W., Rong, P. and Lu, Z., 2009. Snubberless bidirectional DC–DC converter with new CLLC resonant tank featuring minimized switching loss. *IEEE Transactions on industrial electronics*, 57(9), pp.3075–3086.

[27] Moon, S.H., Jou, S.T. and Lee, K.B., 2015. Performance improvement of a bidirectional DC-DC converter for battery chargers using an LCLC filter. *Journal of Electrical Engineering and Technology*, *10*(2), pp.560−573.

[28] Moon, S., Yoon, S.G. and Park, J.H., 2015. A new low-cost centralized MPPT controller system for multiply distributed photovoltaic power conditioning modules. *IEEE Transactions on Smart Grid*, *6*(6), pp.2649−2658.

[29] Dusmez, S., Hasanzadeh, A. and Khaligh, A., 2014. Comparative analysis of bidirectional three-level DC-DC converter for automotive applications. *IEEE Transactions on Industrial Electronics*, *62*(5), pp.3305−3315.

[30] Wu, T.F., Chen, Y.C., Yang, J.G. and Kuo, C.L., 2010. Isolated bidirectional full-bridge DC-DC converter with a flyback snubber. *IEEE Transactions on Power Electronics*, *25*(7), pp.1915−1922.

[31] Duan, C., Wu, D. 2019. Nonlinear voltage regulation algorithm for DC-DC boost converter with finite-time convergence. *Journal of Control Science and Engineering*, pp.1–5.

[32] Salau, A.O., Eya, C.U., Onyebuchi, O.C., 2020 Nonzero staircase modulation scheme for switching DC-DC boost converter. *Journal of Control Science and Engineering*, pp.1–15.

[33] Nguyen, T.V., Aillerie, M., Petit, P., Bui, T.K. 2015. Magnetic dual coupled boost with recovery stage DC-HVDC converter dedicated to renewable. *Energy Procedia journal*, 56, pp. 499–506.

[34] Balbuena, P.B., Wang, Y. (Eds.). Lithium-Ion batteries solid electrolyte Interphase. *Imperial College Press* 2004, ISBN 1-86094-362-4.

[35] Couper, A., 2000. Lead-acid battery desulfator. *Home Power*, 77, pp.84–87.

[36] Nguyen, T.V., Michel, A., Pierre, P., Pham, N.T. and Vo, T.V., 2017. Push-Pull with recovery stage high-voltage DC converter for PV solar. *AIP*, Pari, France, pp. 020058-1-020058-8.

[37] Nguyen, T.V., Pierre, P., Michel, A., Chafic, S., Charle, J.P., 2015. Efficiency of magnetic coupled boost DC-DC converters mainly dedicated to renewable energy systems: Influence of the coupling factor. *International Journal of Circuit Theory and Applications*, 43(8), pp.1042–1062.

[38] Kumar, N., Hussain, I., Singh, B. and Panigrahi, B.K., 2018. Normal harmonic search algorithm-based MPPT for solar PV system and integrated with grid using reduced sensor approach and PNKLMS algorithm. *IEEE Transactions on Industry Applications*, *54*(6), pp.6343−6352.

[39] Safari, A. and Mekhilef, S., 2011, May. Incremental conductance MPPT method for PV systems. In *2011 24th Canadian Conference on Electrical and Computer Engineering (CCECE)*, pp. 000345-000347, IEEE.

[40] Khayyer, P. and Özgüner, Ü., 2014. Decentralized control of large-scale storage-based renewable energy systems. *IEEE Transactions on Smart Grid*, *5*(3), pp.1300−1307.